Optimal gaits for inertia-dominated swimmers with passive elastic joints

Nathan Justus[*] and Ross Hatton[†]

Collaborative Institute for Robotics and Intelligent Systems (CoRIS), Oregon State University, Corvallis, Oregon 97331, USA

Animals and some robots locomote by interacting with the environment through cyclic shape changes, or gaits. Many animals make significant use of passive dynamics with flexible tails or pendulum action to reduce the effort required to execute these gaits. Although geometric tools have been developed to study optimal passive gaits for swimmers in drag-dominated physics regimes, they have not yet been used to study larger-scale swimmers whose physics are dominated by inertial effects. In this paper, we leverage previous work in the geometric mechanics field to examine passive-elastic inertial swimmers and show that geometric mechanics can be used to rapidly determine many classes of optimal gaits for such systems. We also discuss how considering swimmer metabolic costs in addition to the mechanical costs of driving actuation is useful for discussing swimmer efficiency. In particular, we focus on two models of active-passive swimming inertial systems: the perfect-fluid three-link swimmer, and a swimmer with a passively flexible tail.

I. INTRODUCTION

Animals often make use of passive-elastic body elements in their gaits, utilizing flexible tails or pendulum action in the limbs to increase locomotive capabilities. Some fish, for example, have passive properties such that vorticity in a current can excite passive dynamics in the body and cause the fish to "swim" even after the fish has died [1], highlighting the importance of passive mechanical properties in biological locomotion. Humans also exploit passive dynamics while walking: almost no muscle input is supplied to the knee during its swing phase [2].

The geometric mechanics community has developed a range of tools to study the properties of gaits for different locomotor physiologies. Many of these tools, however, assume that the locomotor's shape space is fully actuated such that the system can execute arbitrary gaits, and therefore the tools cannot be directly applied to systems with passive body elements. Although previous works have developed geometric tools for the study of passive systems operating using no-slip constraints [3,4] and for swimming systems operating in drag-dominated regimes [5,6], many systems such as fish or other aquatic systems larger than a few millimeters in length are subject to a different set of dominant physical forces. Such swimmers are better modeled as inertia-dominated systems swimming in a high Reynolds number "perfect fluid," requiring a different mathematical approach [7,8]. In this paper, we construct a methodology for optimizing gaits in inertia-dominated systems with passive-elastic elements that translate and rotate in a plane. We demonstrate that this methodology produces compact equations of motion that allow for simple optimization of gaits that exploit passive dynamics. In

particular, we will discuss two models of simulated active-passive systems, which are assumed to be swimming in a perfect fluid and are illustrated in Fig. 1:

(1) The three-link swimmer, with one passive joint,
(2) A fish-tail swimmer with a passively flexible tail.

For both of these systems, we discuss the properties of optimal motion and the process of passive parameter selection. We show how to select a spring stiffness and damping coefficient that will produce the most favorable passive dynamics for a desired level of mean power consumption from the driving motor given a definition of body geometry. We also discuss how to compare the efficacy of different passive shape modes by observing their respective optimal motions at unit average power exertion from the input joint with properly normalized passive-dynamic coefficients. We demonstrate that the fish-tail swimmer produces more efficient locomotion than the three-link swimmer, indicating that continuous-curvature systems have more favorable locomotive properties.

We then consider the process of optimizing gaits for systems in which the passive dynamic coefficients have already been selected, potentially suboptimally, by material choice or system design. We show that optimizations on both of these swimming systems result in gaits that have similar properties. Optimizing for speed produces a maximum-speed gait that consists primarily of a sinusoid to the active joint. In cases of suboptimal coefficient selection, the input sinusoid can be augmented with a small amount of high-order motion that provides beneficial characteristics in shape space.

Unlike a fully active swimmer, which can move arbitrarily fast when provided with sufficient actuator power, swimmers with fixed passive elements have a single highest-speed gait because of the passive-dynamic interaction. Optimizing for mechanical efficiency produces zero-motion gaits because actuator cost increases faster than displacement as the gait size increases. We demonstrate that considering an additional metabolic cost alongside actuator effort costs, however,

---
[*]justusn@oregonstate.edu
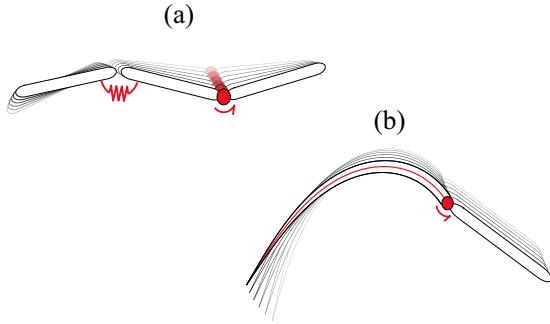[†]hattonr@oregonstate.edu

FIG. 1. The active-passive swimmer models discussed in this paper, shown in motion due to gaits at their passive limit-cycles. Active joints are represented by red circle motors, and passive joints are represented by red springs. (a) The three-link swimmer. (b) The fish-tail swimmer with a passively flexible tail.

produces a class of useful gaits that yield efficient locomotion for systems with varying overhead energy consumption. Low swimmer metabolisms produce minimal motion, as the

swimmer is not incentivized to move quickly. High swimmer metabolisms drive the system to gaits similar to the maximum-speed gait. Middling metabolisms produce gaits that compromise between speed and mechanical costs. High-level optimization results for the three-link swimmer are illustrated in Fig. 2.

II. MATHEMATICAL FORMULATION

In this section, we review the assumptions and techniques that facilitate this work and provide the formulation for the optimization used in our following dynamic system examples. We then briefly discuss techniques for qualitatively understanding the properties of optimal gaits.

A. Obtaining the equations of motion

The models we employ in this paper are built upon the assumption that the momentum of the swimmer-fluid system remains constant throughout the gait cycle [9]—i.e., we only
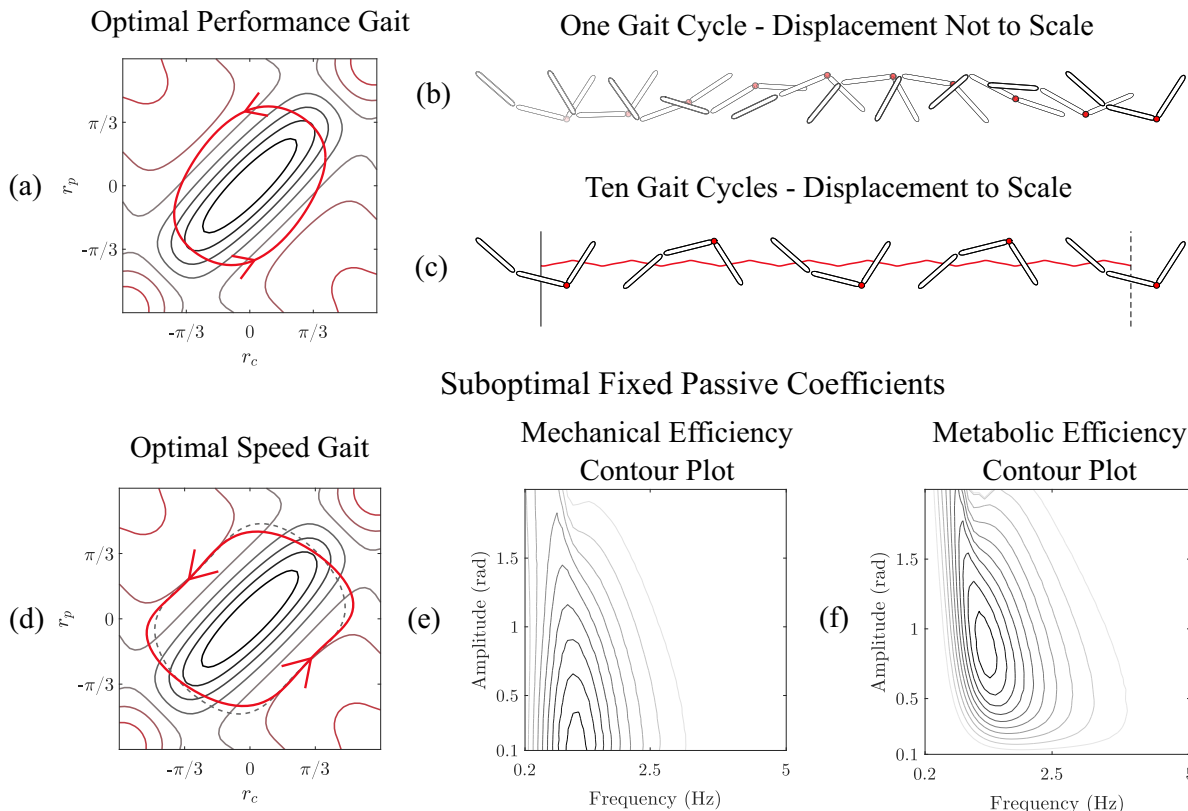

FIG. 2. High-level optimization results for the three-link swimmer: (a) When the passive joint properties can be tuned to suit desired exertion level, the optimal gait is a simple sinusoid input. The gait formed from this input and the passive response is shown superimposed on the forward-motion CCF. (b) The three-link swimmer in the process of its optimal gait, not to scale with swimmer body size. (c) The result of executing ten gait cycles, to scale with swimmer body size. (d) When the passive joint properties are fixed suboptimally and cannot be optimized alongside the gait, the optimal gait includes high order motion on top of the input sinusoid. Gait asymmetry is highlighted with a grey dashed line. (e) A contour plot of mechanical efficiency over various sinusoid inputs to the active joint. Optimizing directly for mechanical power results in zero-amplitude gaits that produce no displacement. (f) A contour plot of metabolic efficiency for a metabolic rate of $\gamma_m = 0.05$. Including metabolic costs alongside mechanical cost of transport in the objective function produces nontrivial efficient optimal gaits.

apply forces to the system through active joint forces, and we do not consider the effects of vortex shedding or fluid drag. This assumption allows us to relate body motion to a system's shape variables r and their time rate of change $\dot{r}$ through the momentum-free *reconstruction equation*,

$$\mathring{g} = \mathbf{A}(r)\dot{r}, \qquad (1)$$

in which $\mathring{g}$ represents swimmer velocity expressed in its local body frame and $\mathbf{A}$ is the *motility map*, which linearly maps shape velocities to the resulting body velocities produced through fluid interaction.[1]

For inertial systems, the motility map can be found by first writing the system's kinetic energy in terms of its body and shape velocity and its generalized mass matrix M,

$$\mathrm{KE} = \frac{1}{2}[\mathring{g}^T \quad \dot{r}^T]M\begin{bmatrix}\mathring{g}\\\dot{r}\end{bmatrix}. \qquad (2)$$

The total mass matrix is formulated from individual link mass matrices μ_i. The individual mass matrices are the sum of mass contributions from both link masses and hydrodynamic added mass terms that take into account the fluid mass that must accelerate with swimmer motion,

$$\mu_i = (\mu_i)_{\mathrm{body}} + (\mu_i)_{\mathrm{fluid}}. \qquad (3)$$

The hydrodynamic added mass plays a key role in the dynamics of swimming systems, as it introduces the anisotropy of reaction forces that allows the systems to generate net position changes through cyclic shape changes.

The individual mass matrices are pulled back into generalized coordinates via the Jacobians J_i relating swimmer velocity and shape velocity to link velocity in the link's frame as in Ref. [8],

$$M(r) = \begin{bmatrix}M_{gg} & M_{gr}\\M_{rg} & M_{rr}\end{bmatrix} = \sum_i \left(J_i^T \mu_i J_i\right). \qquad (4)$$

This mass matrix can be used to intuitively map generalized velocity to generalized kinetic energy as in Eq. (2), and can also be used to map generalized velocity to generalized momentum,

$$p = M\begin{bmatrix}\mathring{g}\\\dot{r}\end{bmatrix} = \begin{bmatrix}M_{gg} & M_{gr}\\M_{rg} & M_{rr}\end{bmatrix}\begin{bmatrix}\mathring{g}\\\dot{r}\end{bmatrix}. \qquad (5)$$

Under the assumption that no mass components are shed from the swimmer, the total momentum of the swimmer-fluid system is conserved. If the swimmer starts at rest, then the system maintains zero position-space momentum for all time. Using this Pfaffian constraint,

$$0 = M_{gg}\mathring{g} + M_{gr}\dot{r}, \qquad (6)$$

we can solve for the motility map $\mathbf{A}$ that maps joint velocities to swimmer body velocities that are consistent with both the specified shape motion and the zero momentum constraint in Eq. (6),

$$\mathring{g} = -M_{gg}^{-1}M_{gr}\dot{r} = \mathbf{A}(r)\dot{r}. \qquad (7)$$

For a closed cyclic gait path ϕ through shape space, total resultant body motion g_ϕ from one gait cycle can be found as the line integral of the motility map along the gait path mapped from the body frame into the system's local coordinates through the body configuration g,

$$g_\phi = \oint_\phi g\mathbf{A}(r). \qquad (8)$$

To estimate the actuator forces required to enforce a desired gait shape, it is useful to represent the swimmer's effective mass in the shape space. This reduced mass matrix M_r can be calculated from the mass matrix and the motility map [8],

$$M_r(r) = [\mathbf{A}^T(r) \quad \mathrm{Id}]M(r)\begin{bmatrix}\mathbf{A}(r)\\\mathrm{Id}\end{bmatrix}. \qquad (9)$$

This formulation allows us to decouple the internal shape-change dynamics from the external body-motion dynamics and write the full system Lagrangian L only in terms of the shape variables without direct consideration of body velocity, because the position-space motion induced by shape change motion is handled implicitly through the motility map. We also take into account passive joint behavior through a stiffness matrix K that encodes the potential energy from passive joint stiffness and a Rayleigh dissipation function G that encodes the damping frictional force at the passive joint through the dissipation matrix B. In this work, stiffness and damping act on the passive shape mode only, and so K and B are zero in the position space terms and can by position-space symmetry be expressed conveniently in the same reduced-dimension space as M_r:

$$L = \mathrm{KE} - \mathrm{PE} = \tfrac{1}{2}\dot{r}^T M_r(r)\dot{r} - \tfrac{1}{2}rKr, \qquad (10)$$

$$G = \tfrac{1}{2}\dot{r}^T B\dot{r}. \qquad (11)$$

When the system shape is composed of a controlled mode r_c and a passive mode r_p such that $r^T = [r_c, r_p]$, the stiffness matrix can be written using only the passive mode spring constant k,

$$K = \begin{bmatrix}0 & 0\\0 & k\end{bmatrix}. \qquad (12)$$

Similarly, for an inertial fluid where the only source of dissipation is damping on the passive joint, the dissipation matrix can be written using only the damping constant b,

$$B = \begin{bmatrix}0 & 0\\0 & b\end{bmatrix}. \qquad (13)$$

Passing the Lagrangian and the Rayleigh dissipation function into the Euler-Lagrange equations produces equations of motion for the system shape variables that account for the dynamics of induced body locomotion and passive joint

---

[1]In previous works, we have used the equation $\mathring{g} = -\mathbf{A}(r)\dot{r}$ and referred to $\mathbf{A}$ as the local connection. Here, to reduce sign confusion, we have included the negative sign in $\mathbf{A}$ and chosen to refer to it as the motility map instead as in Ref. [10].

behavior,

$$\tau = M_r(r)\ddot{r} + C(r, \dot{r}) + Kr + B\dot{r}. \qquad (14)$$

As discussed in our previous work on inertial arts [8], the Coriolis forces can be calculated as

$$C(r, \dot{r}) = \left(\sum_{i=1}^{d} \frac{\partial M_r(r)}{\partial r_i} \dot{r}_i \right) \dot{r} - \frac{1}{2} \begin{bmatrix} \dot{r}^T \frac{\partial M_r(r)}{-\partial r_1} \dot{r} \\ \vdots \\ dot\, r^T \frac{\partial M_r(r)}{\partial r_d} \dot{r} \end{bmatrix}. \qquad (15)$$

Solutions to Eq. (14) for a periodic control joint input signal $r_c(t)$ can be lifted to position-space solutions via the reconstruction equation in Eq. (7) to provide gait limit cycle locomotive properties.

B. Limit-cycle estimation

Our previous work [5] optimizing passive swimming in low Reynolds number systems used Laplace transforms and frequency-space analysis to estimate the passive joint limit cycles. However, this technique is not feasible for inertial systems.[2] In this paper, we estimate the limit cycle by evaluating the ODE from Eq. (14) in the time domain, although others have previously used techniques such as frequency-domain nonlinear harmonic balance methods [3]. Using any of these limit-cycle estimation techniques, we can find signal parameters to the active joint motor that best exploit passive dynamics to suit some objective function. Here, we discuss our time-domain methods.

By separating the shape space into the actively controlled shape mode r_c and the uncontrolled passive shape mode r_p, the equations of motion in Eq. (14) can be rewritten as

$$\begin{bmatrix} \tau_c \\ -kr_p - b\dot{r}_p \end{bmatrix} = \begin{bmatrix} M_{cc}(r) & M_{cp}(r) \\ M_{cp}(r) & M_{pp}(r) \end{bmatrix} \begin{bmatrix} \ddot{r}_c \\ \ddot{r}_p \end{bmatrix} + \begin{bmatrix} C_c(\dot{r}, r) \\ C_p(\dot{r}, r) \end{bmatrix}. \qquad (16)$$

To simulate these dynamics, we write the active joint control signal as an nth-order Fourier function of time parameterized by the Fourier variables $a_{0...n}$, $b_{1...n}$, and ω,

$$r_c(t) = a_{c,0} + \sum_{i=1}^{n} (a_{c,i} \cos(i\omega t) + b_{c,i} \sin(i\omega t)). \qquad (17)$$

By taking time derivatives of this equation, the joint velocities $\dot{r}_c$ and joint accelerations $\ddot{r}_c$ can be readily calculated. These values are used to numerically solve for the configurations of the passive modes over time by solving Eq. (16) for $\ddot{r}_p$ and evaluating the resulting ODE,

$$\ddot{r}_p = M_{pp}^{-1}(-kr_p - b\dot{r}_p - M_{cp}\ddot{r}_c - C_p). \qquad (18)$$

---

[2]In our previous work, we approximated that the drag matrix is constant, which allowed us to perform Laplace transforms and directly estimate the passive transfer function. For inertial systems, the mass matrix is heavily dependent on the swimmer shape, so the assumptions required for Laplace domain analysis are no longer valid. Additionally, assuming a constant mass matrix eliminates our ability to factor in centrifugal and Coriolis forces, as these are calculated from mass matrix derivatives.

We estimate limit cycle shape motion by finding the behavior that results from multiple executions of the candidate control signal. We then estimate gait displacement by using the local connection relationship in Eq. (7) to calculate the net motion that results from limit cycle execution of the gait. In Sec. III, we will use the properties of this limit cycle such as net displacement, gait cost, and gait period to evaluate the fitness of a candidate control signal and perform optimizations over control signal parameters and passive shape properties.

C. Mechanical cost of transport

Once the gait limit cycle is known, we can also find the energy consumption required to enact this gait. In this work, we use positive mechanical power as the primary source of energy consumption, representing the energy required by the control motor to enforce the desired shape motions over the course of the gait period T. The control joint requires no energy input when backdriven during periods of negative mechanical power [11]. The mechanical cost of transport E_τ is the total positive mechanical power usage over the gait,

$$E_\tau = \int_0^T \max(\tau_c \dot{r}_c, 0) dt. \qquad (19)$$

Here, the c subscript refers to the fact that we only consider power consumed by the control joint, as passive joint mechanical power comes for free from the passive components.

We will use the notion of control motor power consumption in later sections of the paper to discuss gait efficiency in terms of displacement with respect to the mechanical cost of transport.

D. Gait intuition through the constraint curvature function

The motility map **A** is a covector field over the shape space mapping shape space motions to body motions. Net gait displacement can be found by integrating the motility map over the path of the gait ϕ while mapping instantaneous motion from the body frame into the world frame through the swimmer state g as in Eq. (8). If the gait shape motion is a closed loop, then this line integral can be approximated by an area integral over the enclosed space ϕ_a in a manner similar to Stokes' theorem [12],

$$g_\phi = \oint_\phi g\mathbf{A}(r) \approx \iint_{\phi_a} D\mathbf{A}, \qquad (20)$$

where $D\mathbf{A}$ is the curvature of the constraints encoded by **A**. This constraint curvature function (CCF) is generally useful for examining regions of the shape space that contribute to locomotion in the desired direction [12]. Gaits are more effective at achieving displacement if they enclose sign-definite regions of the CCF. The forward-motion CCF for the three-link swimmer is shown in Fig. 2(a).

This approximation is most accurate in body coordinates at a generalized center of mass. These coordinates minimize the noncommutative interactions from the intermediate motions along the gait [13].

In this work, we use the motility map to directly measure the net motion from gait limit cycles as in Eq. (8) and the CCF to provide high-level intuition into why optimal gaits tend to
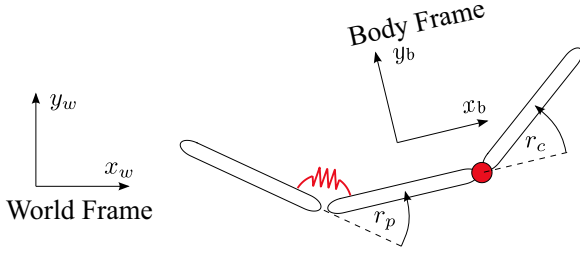
FIG. 3. Shape parametrization of the three-link swimmer.

develop particular shapes. Speedy and efficient gaits will generally enclose primarily the positive black region in the center while minimizing the amount they enclose the surrounding negative red regions.

E. Swimmer modeling

To demonstrate the principles described above, we apply them to two swimming locomotors.

The first is the three-link swimmer, a model that is commonly used as a minimal reference example for locomoting systems [14]. As illustrated in Fig. 3, the three-link swimmer is composed of a chain of three elongated links, and the swimmer shape is parameterized by the angular deflection of the two joints in the chain. By performing the geometric process detailed above, the low Reynolds number Purcell swimmer can be modified into a perfect-fluid swimmer in an idealized high Reynolds number environment. To model hydrodynamic added mass, we approximate each link as an ellipse and use added mass coefficients given for ellipses in previous works [15]. To simplify the process, we assume that each swimmer element has a constant hydrodynamic mass, although a full shape-dependent, hydrodynamically coupled model could be found using the panel method [7] at some additional computational expense.

The second system is the fish-tail swimmer, which has a passively flexible tail. Continuously flexible systems are common in aquatic locomotion, as biological swimmers tend to locomote using motions that continuously deform the body rather than with joint-like behavior [16,17]. Aside from the flexible tail, this model is conceptually similar to the three-link swimmer, with oscillations of a rigid "head" driving locomotion. The fish-tail swimmer is illustrated in Fig. 4.
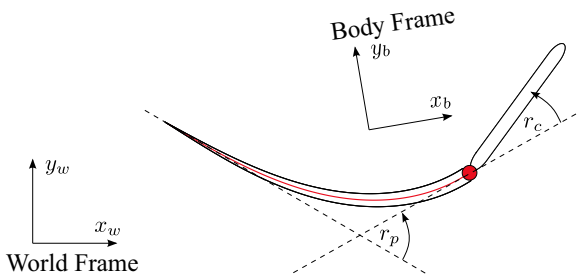

FIG. 4. Shape parametrization of the fish-tail swimmer. The passive shape mode is tuned so that the shape magnitude is equal to the angular deflection at the tip of the tail.

In this work, we simplify the model of a continuously flexible tail by assuming that tail stiffness is high enough that the forcing frequency is below the fundamental eigenfrequency, so all motion corresponds to the first mode of an inertial cantilever beam. Curvature of the tail is at a maximum where it connects to the swimmer head, and decays to zero at the tip of the tail.

To estimate the curvature mode of the passive-flexible tail, we take the tail as an Euler-Bernoulli beam of tapering width. Using beam theory, we find the relationship between the curvature of the tail and the force profile applied along the length. Using this curvature-force relationship, we iterate until we find a curvature mode consistent with the inertial force profile that results from that modal acceleration.

We initially model the force profile on the beam as the force on a straight beam undergoing angular acceleration through fluid at the base of the tail. We model the inertial force $f(s)$ on the rigidly rotating beam as linearly decreasing along the tail arclength s from a maximum at the beam tip ($s = 0$) to zero at the base of the tail ($s = 1$) due to the acceleration of the beam components through the fluid,

$$f(s) = f_0(1 - s). \tag{21}$$

The particular force magnitude f_0 is not important at this point because we will later rescale the shape parametrization such that the mode has unit integrated curvature. We then analytically solve for the internal moment $m(s)$ at each point along the beam that gives balance to the applied inertial forces,

$$m(s) = \frac{f_0}{2}\left(s^2 - \frac{s^3}{3}\right). \tag{22}$$

To approximate the continuous stiffness of a biological fish, we use a tapered body profile, such that beam moment of inertia $I(s)$ is at a maximum where it connects to the "head" and decays to zero at the tail tip,

$$I(s) = I_0 s. \tag{23}$$

The moment of inertia profile combined with the elastic modulus E gives a local bending stiffness $k(s)$ for each point along the beam arclength that relates the internal moment at that point to the resultant local curvature κ_e based on the beam mechanical properties,

$$k(s) = EI(s) = \frac{m(s)}{\kappa_e(s)}. \tag{24}$$

Using the local stiffness profile given by the tapering beam shape and the internal moment profile found from the force distribution, we can calculate the resulting curvature profile over the beam,

$$\kappa_e(s) = \frac{m(s)}{k(s)} = \frac{f_0}{2EI_0}\left(s - \frac{s^2}{3}\right). \tag{25}$$

To ensure convergence of the iterative algorithm, we enforce through a scaling factor C that each iteration of the curvature mode has unit amplitude,

$$C\int_0^1 \kappa_e(s)ds = 1. \tag{26}$$

This gives a normalized shape mode curvature profile in terms of the passive shape magnitude r_p,

$$\kappa_p(s) = C\kappa_e(s)r_p. \tag{27}$$

A convenient side-effect of normalizing the curvature mode is that it leads to shape magnitudes r_p that are directly comparable to those of the three-link swimmer. With this normalization, the tip orientation associated with a particular shape magnitude aligns with the orientation of the three-link swimmer tail at the same magnitude. This correspondence of tip angle to a discrete joint on the swimmer is illustrated in Fig. 4.

Once we have this shape mode, we replace the force profile used in Eq. (21) with the inertial force profile that would result from acceleration of this curvature mode,

$$f_{n+1}(s) = f_0 \int_0^s (s - \ell)\kappa_p(\ell)d\ell, \tag{28}$$

where ℓ is an intermediate variable that allows for integration along the arclength up to the specified location s. We then iterate these calculations, using forces to estimate curvatures and curvatures to estimate forces, until the shape mode converges to a curvature profile consistent with inertial forces that would result from that profile. We use the converged curvature profile as our mode-shape for low-dimensional analysis.

This passive shape mode approximates the deflections experienced by a tapered beam in inertial fluid where the forcing frequency serves to excite primarily the first eigenmode, which has been previously shown to be an effective way of producing reactive thrust for slender metal beams submerged in water [18]. Subsequent modes can be added to generate traveling waves and more complex passive behavior.

Once we have a curvature profile for the shape mode, we can calculate the Jacobian $J(r, s)$ continuously along the beam arclength using techniques presented in our previous works [19]. The mass metric contribution from the tail is calculated akin to Eq. (4) by integrating the hydrodynamic mass pullback along the beam using the beam's hydrodynamic mass density ρ_m,

$$M(r) = J_h(r)^T \mu_h J_h(r) + \int_0^1 J(r, s)^T \rho_m J(r, s)ds, \tag{29}$$

where the h terms represent the mass metric contribution from the rigid head element.

Beam stiffness can be expressed in the shape mode as the second derivative of tail potential energy with respect to the passive shape mode deformation. Integrating along the tail to find the potential energy, we find

$$\text{PE} = \int_0^1 \frac{1}{2}k(s)\kappa_p^2(s)ds. \tag{30}$$

From here we calculate the modal stiffness,

$$k_p = \frac{\partial^2 \text{PE}}{\partial r_p^2} = C^2 \int_0^1 k(s)\kappa_e^2(s)ds. \tag{31}$$

The modal stiffness k_p is a spring constant that relates shape mode magnitude to the net beam passive response due to the beam mechanical properties, and can be used to build the stiffness matrix in Eq. (12).

TABLE I. Generalized units for quantities used in this work.

Described quantity	Symbol	Unit
Swimmer Length	ℓ	ℓ
Time	t	s
Mass	m	m
Net Gait Displacement	D	ℓ
Gait Period	T	s
Gait Frequency	Hz	$1/T \rightarrow 1/s$
Instantaneous Body Velocity	$\mathring{g}$	ℓ/s
Gait Speed	η_v	$D/T \rightarrow \ell/s$
Shape Deflection	r	rad
Shape Velocity	$\dot{r}$	rad/s
Shape Acceleration	$\ddot{r}$	rad/s^2
Torque	τ	$m\ell^2/s^2$
Spring Stiffness Coefficient	k	$\tau/r \rightarrow m\ell^2/rads^2$
Damping Coefficient	b	$\tau/\dot{r} \rightarrow m\ell^2/rads$
Energy	E	$m\ell^2/s^2$
Power	P	$E/s \rightarrow m\ell^2/s^3$
Metabolic Rate	γ_m	$E/s \rightarrow m\ell^2/s^3$
Mechanical Efficiency	η_τ	$D/E \rightarrow s^2/m\ell$
Metabolic Efficiency	η_m	$s^2/m\ell$

Previous works have investigated limit cycle estimation for locomotors with multiple passive modes [3], allowing for the optimization techniques presented in this work to extend to systems with additional passive shape modes. If given physical motion data for points along a flexible body moving in fluid, then appropriate shape modes can be extracted using the technique of eigenvector analysis [20]. This allows for a model to be built with behaviors that more closely resemble physical motion of a desired system.

F. Units

The numerical results we present later in the paper use the set of units provided in Table I.

III. OPTIMIZING PERFORMANCE

In general our high-level optimization process is as follows. First, we choose a swimmer model and use this model to develop passive-dynamic equations of motion. Then, we can estimate the whole-body limit-cycle that results from a particular choice of control joint input signal $r_c(t)$ and passive joint parameters k and b. Net gait motion is found by integrating the motility map over the gait cycle, gait period is found from the gait frequency parameter, and gait energy cost due to actuator usage is found by integrating actuator effort over the gait cycle. These metrics are combined into a fitness function that quantifies the performance of a choice of control joint input signal and passive parameters. The input signal and passive joint parameters can then be optimized for the chosen objective function using any sample-based optimization algorithm.

Depending on whether we are optimizing the gaits of a fixed physical plant or simultaneously optimizing gaits alongside physical design, there are multiple possible routes for optimizing passive-inertial systems.

If the optimization is performed before the system is fully instantiated, then the spring and damping constants can be chosen alongside the gait parameters to optimize system behavior and the passive dynamics with respect to a desired average level of energy exertion. This method can be used to compare the performance of potential locomotor geometries or shape modes by comparing ideal performance of the different systems under identical power consumption.

It is also possible to optimize gaits for systems that have immutable passive coefficients that cannot be optimized alongside the gait parameters. This route is more applicable to systems where the passive coefficients are fixed in place by material choice or other design considerations.

In this section, we will describe how we construct the objective functions that we use to optimize gaits for the separate cases of mutable and immutable passive joint behavior.

A. Simultaneously optimizing gaits and passive coefficients

The systems we deal with in this paper are heavily nonlinear, with the system mass matrix and subsequent limit-cycle dynamic behavior being strongly coupled to shape space. However, once a limit-cycle transfer function for a given input motion is established using nonlinear methods, we can use a linear approach to find a curve through the space of joint properties and actuator frequency that produces constant transfer functions. Along these particular identical-transfer-function curves in parameter space, nonlinear effects scale cleanly because there are no variations in the gait's path and relative pacing. For these cases, scaling from linear theory is exactly correct even on the nonlinear system. These curves can be monotonically parameterized by input power to the active joint, so we can select a point along it to match the available power. The optimization problem then becomes finding the highest-speed limit cycle that can be executed at unit power. After finding this pairing of optimal unit-power input motion and passive parameters that enable this motion, the behavior can be scaled to any desired average power level using linear theory, giving simultaneously the fastest and most efficient locomotion possible at that power level.

Our identical-transfer-function curves are formed in the space of three parameters: the spring constant k, the damping constant b, and the gait frequency ω. For the limit cycle transfer function to stay the same, two ratios must be preserved: The first is the ratio of the input frequency to the system's natural frequency,

$$R_\omega = \frac{\omega}{\omega_n} = \frac{\omega}{\sqrt{k/m}}, \qquad (32)$$

and the second is the damping ratio,

$$\zeta = \frac{b}{2\sqrt{km}}. \qquad (33)$$

In the space of our three parameters k, b, and ω, the frequency ratio and damping ratio act as two constraints that enforce a constant limit-cycle transfer function. This leaves us with a one-dimensional curve through the parameter space on which the transfer functions will be identical for the same input motions. Along the identical-transfer-function curve, the two ratios are constant, so along the curve the spring constant is

proportional to ω^2 and the damping constant is proportional to ω (neglecting variations in mass because they will be identical along the curve). This means that we can parametrize the constant-transfer-function curve as a function of gait frequency,

$$TF(\omega) = (k(\omega), b(\omega), \omega) = (k_0\omega^2, b_0\omega, \omega), \qquad (34)$$

in which k_0 and b_0 are the spring and damping constants corresponding to unit gait frequency.

For the system effort, we consider primarily the positive mechanical power,

$$P_c = \max(\tau_c \dot{r}_c, 0), \qquad (35)$$

representing the rate of energy supply required to enforce actuator motions. An actuator without regenerative braking will consume energy during periods of positive mechanical power and will require no energy when backdriven during periods of negative mechanical power [11].

Examining time-derivatives of the Fourier parametrization expressed in Eq. (17), we observe that input speed across the gait $\dot{r}_c$ is proportional to ω and input acceleration $\ddot{r}_c$ is proportional to ω^2. We also note from the dynamic equation of motion expressed in Eq. (14) that control torque τ_c is proportional to input acceleration. Combining these relationships in Eq. (35), we see that the average positive mechanical power supplied to the control motor is proportional to ω^3 along the constant-transfer-function curve. This relationship is formed as

$$P_{\text{avg}} = P_0\omega^3, \qquad (36)$$

where P_0 is the average power required to execute the gait when performed at unit gait frequency. From this power-scaling relationship, we can solve for the gait period that would result in a unit-power execution of the given limit cycle:

$$T_1 = P_0^{1/3}. \qquad (37)$$

The corresponding unit-power gait frequency comes from the simple inverse relationship between period and frequency,

$$\omega_1 = \frac{1}{T_1}. \qquad (38)$$

This relationship lets us avoid the computationally difficult nonlinear constraint of directly restricting gaits to unit power. Instead, we fix the gait frequency to unit value, observe the power required to enact the limit cycle for given passive parameters and gait definition coefficients, and then find the gait frequency and passive parameters that give the same limit cycle in shape space at unit power consumption.

In summary, we can optimize the physical parameters that determine the passive dynamics alongside the control parameters that define the gait. To do this, we fix gait frequency to unit value, leaving the remaining optimization variables as the Fourier parameters, stiffness coefficient, and damping coefficient. To perform our optimization, we simulate the passive-dynamic response to the described input motion and observe the limit-cycle energy cost E_τ and the net forward displacement D that result. From the unit-period energy cost, we find the gait period and passive coefficients that result in unit-power execution of the same limit cycle with the same
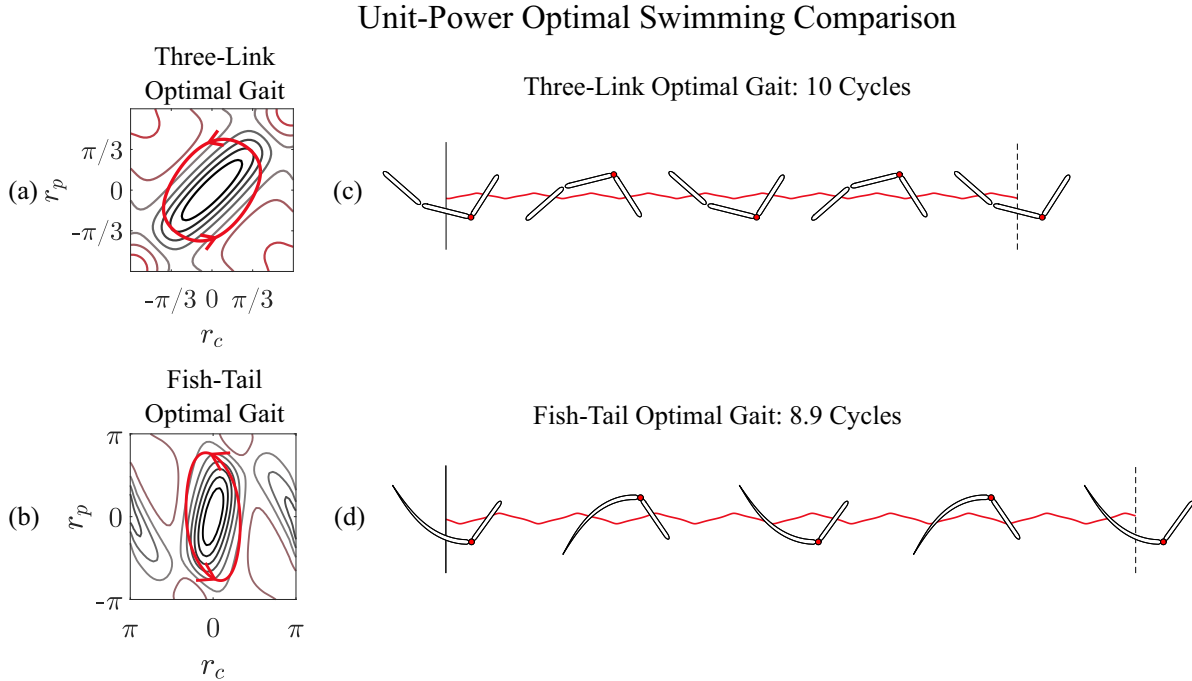
Unit-Power Optimal Swimming Comparison

FIG. 5. Comparison of the three-link swimmer and the fish-tail swimmer with optimized passive coefficients performing their optimal gaits at unit power consumption. Although the three-link swimmer can perform its gait 10% faster than the fish-tail swimmer at unit power, the displacement per gait cycle is substantially lower, so the fish-tail swimmer has more efficient locomotion overall. (a) The three-link optimal gait superimposed on the forward-motion CCF. Optimal motion for tuned passive parameters is a simple sinusoid input. (b) The fish-tail optimal gait superimposed on the forward-motion CCF. Optimal motion for tuned passive parameters is a simple sinusoid input. (c) Result of the three-link swimmer performing 10 gait cycles at unit power consumption, with displacement to scale with swimmer body. Body center-of-mass tracked with a red background line. (d) In the time it takes the three-link swimmer to perform 10 gait cycles at unit power, the unit-power fish-tail gait can be performed only 8.9 times. Result of the fish-tail swimmer performing 8.9 gait cycles, with a red background line tracking body center-of-mass motion.

gait parameters. Our objective function is then the locomotor speed when the gait is executed at unit power,

$$\eta = \frac{D}{T_1}. \tag{39}$$

The gait that maximizes speed given unit power input can be rescaled using Eqs. (34) and (36) to find the frequency and passive parameters that produce the fastest and most efficient locomotion at any desired power budget.

Results for optimizing gaits and passive parameters for the three-link swimmer and the fish-tail swimmer are shown in Fig. 5. Both optimal gaits consist of first-order sinusoids. We attribute the lack of high-order motion to the fact that high-order joint activity comes with cubicly increasing power costs.

Comparing the behavior of the two systems at unit average power consumption of the driving motor, we can see that the fish-tail swimmer is approximately 20% more efficient than the three-link swimmer. Although the three-link swimmer can perform its optimal gait 10% faster than the gait of the three-link swimmer, its displacement per cycle is only 75% of that of the three-link swimmer. It is likely that other choices of body curvature could improve the performance of the fish-tail swimmer even further. Unlike the fish-tail model, migratory biological swimmers like trout and salmon produce efficient long-distance locomotion through body curvature that is heavily concentrated towards the rear of the swimmer [21]. The tapering-stiffness beam, however, develops a high curvature

concentration near the center of the swimmer body, leading to potentially suboptimal behavior.

B. Objective functions for fixed suboptimal passive coefficients

For a robot, it is not always the case that we have full control over the passive parameters of body stiffness and damping. These factors are likely to be influenced by material choice in the body of the locomotor or other considerations in mechanical design. For these cases, we seek to find the input joint behavior that produces best locomotion given an existing physical system.

With fixed passive behavior, we can no longer rescale the stiffness and damping coefficients to shift an arbitrary passive-dynamic limit cycle to any desired input frequency. Under this condition it no longer makes sense to restrict gaits to unit power consumption, because behavior will not scale cleanly over different power budgets. For fixed-coefficient swimming systems, we must therefore define a new set of objective functions.

The first of these objective functions is the locomotor speed,

$$\eta_v = \frac{D}{T}, \tag{40}$$

where D represents the net forward displacement of the swimmer per gait cycle and T is the gait period. This quantity gives

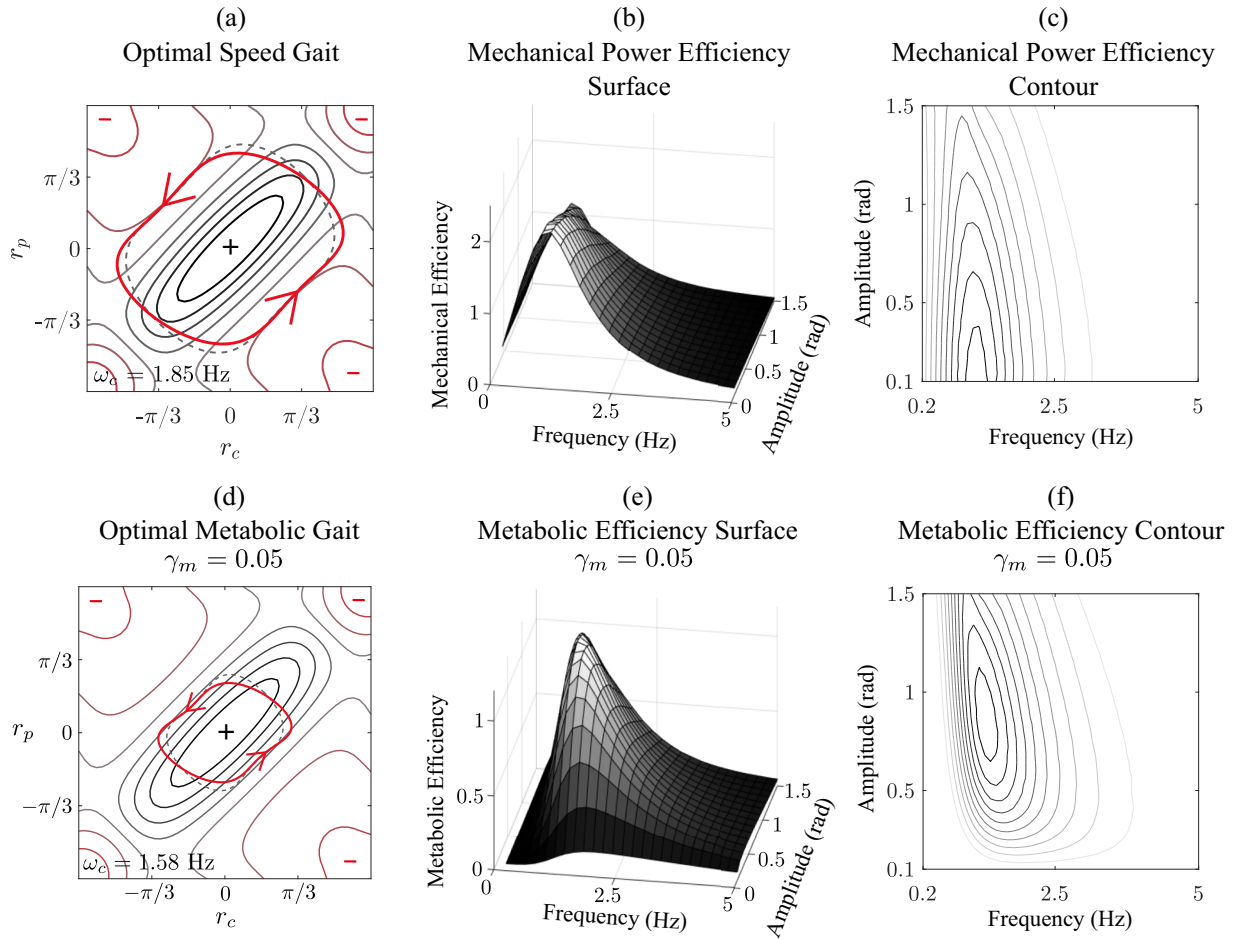## Three-Link Swimmer Optimal Gaits: Suboptimal Passive Components

FIG. 6. Results for the suboptimally tuned passive three-link swimmer across our three objective functions: (a) The maximum-speed gait superimposed on the forward-motion CCF. With fixed passive coefficients, optimizing for speed results in a single best gait with frequency dependent on the passive parameters. The gait uses high-order motion at the active joint to compensate for poor passive-properties, resulting in asymmetric motion. Asymmetry highlighted using a symmetric grey dashed line. (b), (c) Mechanical efficiency of the passive three-link swimmer at various input sinusoids for the mechanical power objective function. Considering only mechanical power costs without fixing a power budget results in an optimal gait with near zero input motion. (d) Results for optimizing a gait while taking into account a metabolic energy drain rate of $\gamma_m = 0.05$. Considering metabolic costs causes the optimizer to compromise between speed and energy expenditure. (e), (f) Locomotive efficiency of the passive three-link swimmer when considering metabolic drain. Taking into account energy overhead for the swimmer results in a nontrivial optimal gait even without constraining the optimization to a power budget.

a measure of how far the swimmer will travel using a certain gait in unit time.

For our second optimization function, we choose mechanical efficiency,

$$\eta_\tau = \frac{D}{E_\tau}. \tag{41}$$

By dividing gait displacement by the energetic cost, we find how far the swimmer can travel per unit energy sent to the control motor.

The final objective function takes into account both actuator power consumption and other miscellaneous energy overhead via a metabolic rate γ_m that represents the rate of time-dependent energy expenditures, such as processor power

consumption:

$$\eta_m = \frac{D}{E_\tau + \gamma_m T}. \tag{42}$$

C. Results of optimization

In the following text, we discuss the results of optimizing passive gaits on our two swimmers when passive coefficients are frozen at arbitrary suboptimal values. In particular, we used a stiffness coefficient of 0.075 and a damping coefficient of 0.01 for both systems. We first discuss the effects of optimizing each of our three objective functions on both systems. Unlike fully actuated swimmers, which can locomote arbitrarily fast, passive swimmers have a bounded maximum speed because of the passive-dynamic interaction. Moving at too high a frequency produces straight-line gaits in shape space that produce no net locomotion [5]. The maximum speed gait

for both systems consists of an active joint input at a moderate frequency that is predominantly a first-order sinusoid with small high-order augmentations that provide beneficial characteristics in the shape space. Optimizing for efficiency with respect to actuator energy expenditure produces trivial zero-motion gaits that would cause swimmers to take infinite time to traverse between any two points. Adding metabolic considerations to the energy expenditure cost produces a range of nontrivial efficient gaits.

We then discuss how allocating a power budget affects optimal motion for swimmers with fixed passive coefficients. We see that increasing budgets for mechanical power expenditure allows for increased gait frequency and input motion magnitude. Beyond the budget required for the maximum-speed gait however, there are no benefits to increasing the power budget because it is not possible for the system to move faster with the additional energy.

1. Speed

The fixed-coefficient passive swimmers each have a bounded upper limit on speed, even with an unbounded power budget, because of the passive dynamics between the active and passive joints [5]. At high input frequencies, the passive response phase lag shifts so that there is very little resultant net motion.

Results for optimizing swimmer speed are illustrated in Fig. 6(a) for the three-link swimmer and in Fig. 8(a) for the fish-tail swimmer. Both have very similar characteristics. The optimizer tends to converge towards a predominantly sinusoidal input with a small amount of high-order motion. The high-order motion compensates for the imperfect tuning of the passive parameters by "flicking" the passive tail and achieving beneficial characteristics in shape space. The contribution of high-order motion to the optimum-speed gait for the three-link swimmer is shown in Fig. 7. This additional high-frequency motion is rather expensive, however, requiring a large amount of energy to be supplied to the actuator, and disappears from optimal results as the power budget is reduced.

For the arbitrary suboptimal coefficients we chose, the optimizer found the optimal gait frequency to be approximately 1.85 Hz for the three-link swimmer and 1.95 Hz for the fish-tail swimmer. These optimal frequencies depend on the particular passive coefficients that are chosen for each system alongside the shape-mode description. Because of the different mechanics of the passive-elastic components, the only way to "fairly" compare these two shape modes is by using the equal-power optimally tuned results given in Fig. 5.

For the suboptimal passive coefficients we chose, the three-link maximum-speed gait locomotes at approximately 80% of the speed of the optimal-coefficient gait when the latter is performed at the same level of power exertion. For the fish-tail swimmer, the fixed-coefficient optimal-speed gait locomotes at roughly 75% of the speed of the corresponding optimal-coefficient fish-tail gait.

2. Mechanical efficiency

Optimizing for gaits that are efficient with respect to the mechanical cost of transport does not produce motions that would be useful for physical swimmers. The optimizer

Effect of Adding High-Order Terms To Three-Link Optimal Speed Gait
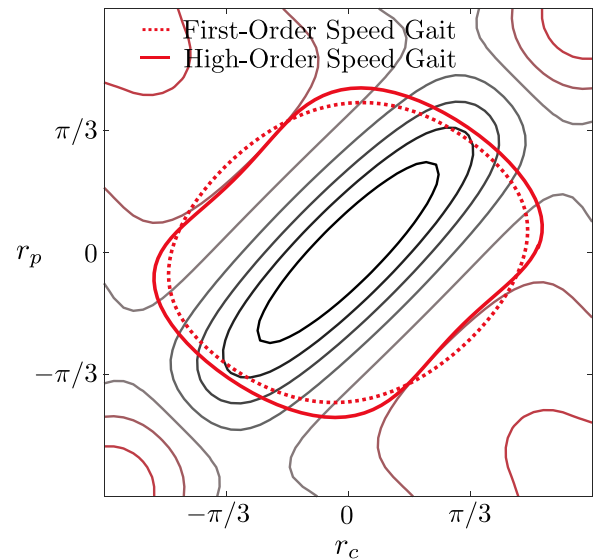

FIG. 7. Effect of adding high-order terms to the fixed-coefficient optimal speed gait for the three-link swimmer: The optimal speed gait is shown (red line) superimposed on the forward-motion CCF (contour plot) alongside the effects of performing only the first-order terms of the same gait (red dotted line). The high-order terms aid the gait by slightly extending the gait along the positive-motion black diagonal area of the CCF while reducing the amount the gait enters the negative-motion red area.

converges to asymptotically zero amplitude, producing zero-motion gaits that would take infinite time to traverse between any two points. This lack of motion is because power consumption increases more quickly than locomotive distance as active joint motion increases. Figures 6(b), 6(c) and 8(b), 8(c) show mechanical efficiency across input sinusoid amplitudes and frequencies for both the three-link swimmer and fish-tail swimmer. Both efficiency surfaces indicate that minuscule gaits produce the most efficient motion when considering only actuator energy costs. For real-world swimmers, such low-motion gaits would produce negligible locomotion speeds and would not be useful for real-world applications. We can, however, indirectly optimize for mechanical efficiency by allocating a power budget and finding the highest speed possible that makes use of that budget. Performing this optimization across multiple power budgets results in a Pareto frontier of gaits across the dual objective functions of power expenditure and speed. We will discuss results of this process in Sec. III D.

3. Metabolic efficiency

Physical implementations of these swimming systems will have continuous sources of energy loss other than the actuator, such as processor power consumption. These metabolic costs can be included into the energetic efficiency by introducing a component that scales with the metabolic rate γ_m and the gait time period T. This produces a new metabolic energy objective function that encourages the optimizer to find gaits that balance speed and energy costs. This objective function,

Fish-Tail Swimmer Optimal Gaits: Suboptimal Passive Coefficients
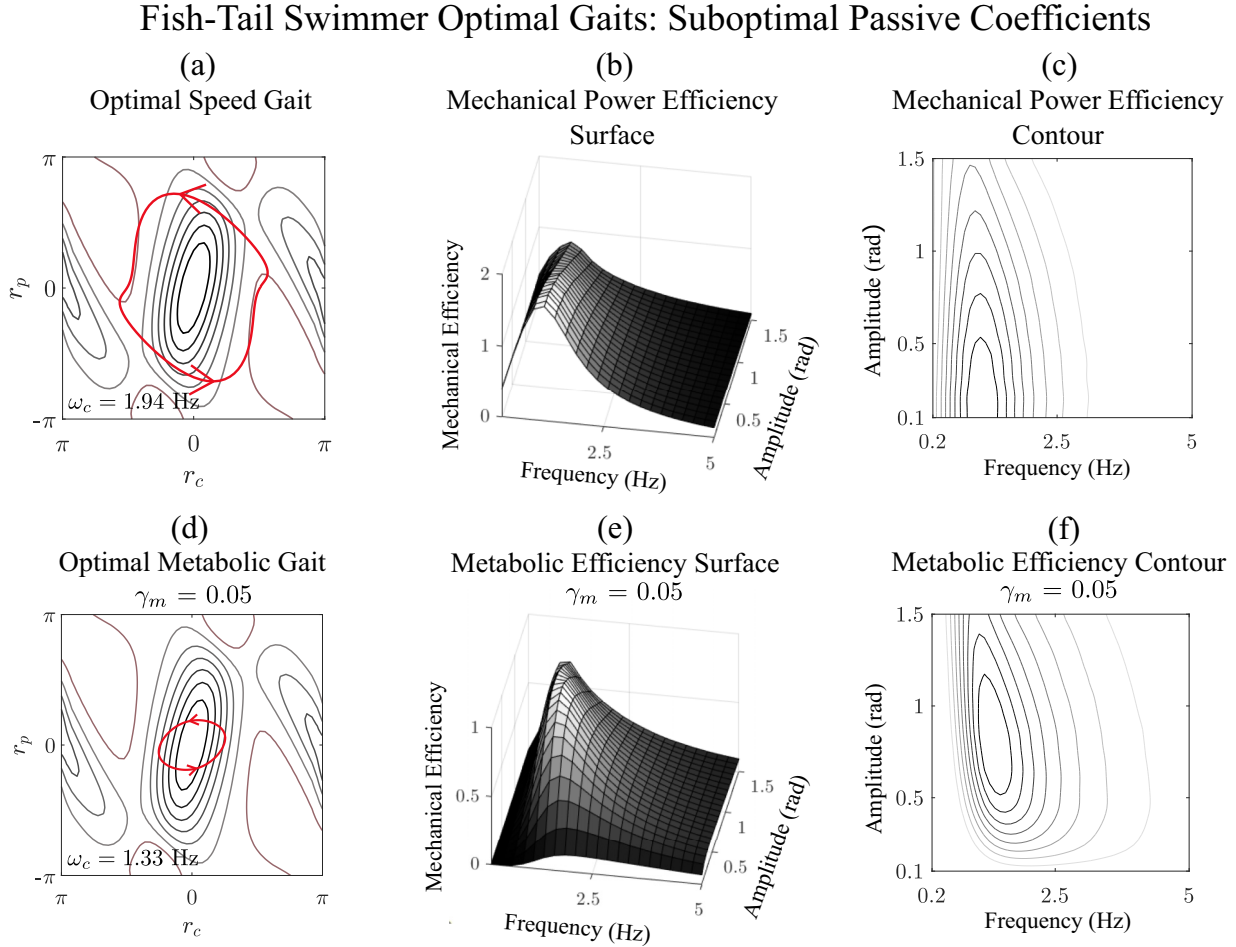

FIG. 8. Results for the passive fish-tail swimmer across our three objective functions: (a) The maximum-speed gait (superimposed on the forward-motion CCF), which consists of a large sinusoid input augmented with a small amount of high-order motion that widens the gait in shape-space. (b), (c) Locomotive efficiency of the passive fish-tail swimmer at simple input sinusoids for the mechanical power objective function. Considering only mechanical power costs results in an optimal gait with near zero input motion. (d) Results for optimizing a gait while taking into account a metabolic rate of $\gamma_m = 0.05$. (e), (f) Locomotive efficiency of the passive fish-tail swimmer when considering metabolic drain. Taking into account energy overhead for the swimmer results in a nontrivial optimal gait.

expressed in Eq. (42), allows for efficiency optimizations that produce meaningful results.

Optimizing with this new objective function produces results that change alongside the metabolic rate. When the swimmer metabolism is near zero, optimizations converge towards low displacement gaits that prioritize reduction of actuator effort over actual locomotion, giving results similar to mechanical efficiency optimization. For swimmers with very high metabolic costs, the time-scaling term dominates the energy consumed by the active joint and the swimmer is encouraged to find speedy gaits. Such optimizations produce speed-optimal gaits like those shown in Figs. 6(a) and 8(a). Middling metabolism values, where metabolic costs rival transport costs and neither of the terms dominate, produce gaits that compromise between these two extremes. An example of such a metabolic gait is illustrated in Fig. 6(d) for the three-link system and in Fig. 8(d) for the fish-tail system. By optimizing for a metabolic rate $\gamma_m = 0.05$, we find a nontrivial optimal gait for each system that is much more energetically efficient than the max speed gait. Figures 6(e), 6(f) and 8(e), 8(f) show metabolic efficiencies for the two swimmers across

different sinusoidal inputs. Unlike the mechanical power objective function shown in Figs. 6(b), 6(c) and 8(b), 8(c), the metabolic objective function results in nontrivial optimal gaits even without mandating a minimum energy expenditure.

D. Effects of allocating power budgets

In our previous work [8] we found efficient gaits by allocating an energy budget and finding the highest-speed gait that made use of this budget. The methodology of optimizing for speed given a power budget rather than directly for mechanical efficiency produces a single nontrivial gait that both maximizes speed-at-power and minimizes power-at-speed. For the fully active problem this most-efficient gait gives the optimal solution at any desired power level by a simple timescaling of the same path through shape space. As we showed in Sec. III A, this timescaling property of the optimal gait across all power budgets can be extended to passive systems with mutable passive coefficients by rescaling the system stiffness and damping alongside the gait frequency. This solution is less simple for passive systems with prede-

Effects of Constraining Frequency and Maximum Average Power Exertion
Fixed-Coefficient Three-Link Swimmer

Best Possible Speeds
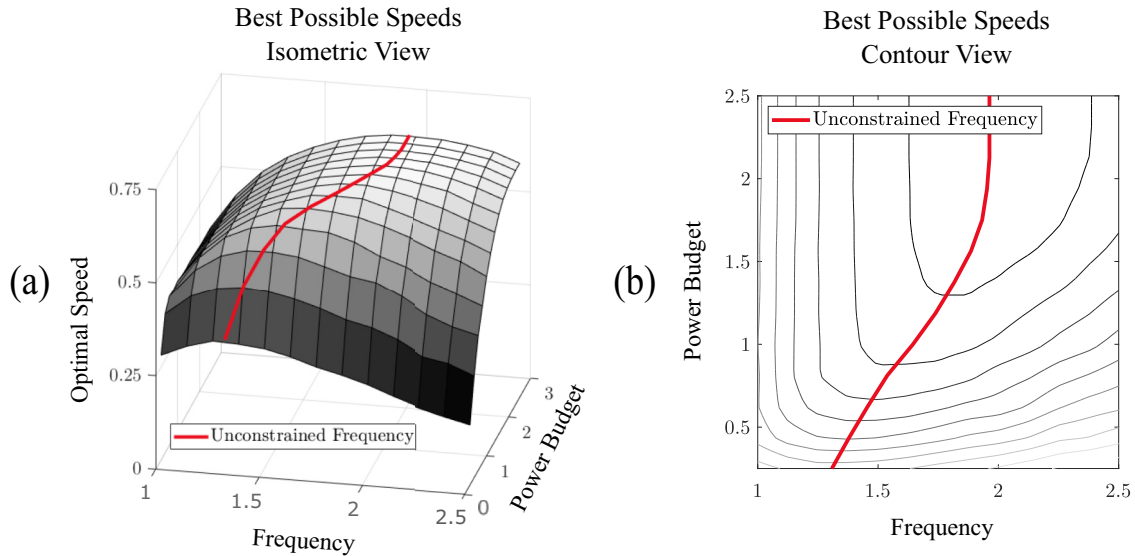Isometric View

Best Possible Speeds
Contour View

FIG. 9. Optimal speed behavior over various power budgets and gait frequencies for the fixed-coefficient three-link swimmer. (a) Surface plot of optimal gait speeds over input power budgets and gait frequencies. Each node represents an individual gait speed optimization problem at a constrained level of maximum average power consumption and constrained input frequency. The red line represents the Pareto frontier that results from relaxing the frequency constraint in the optimizations. Over this Pareto frontier, gait speed trades off with power consumption. (b) Contour map of the same plot. Optimal frequency and gait speed increases with increasing power budget until the global maximum speed gait can be executed, after which there is no benefit or change in behavior from increasing power budget.

termined immutable coefficients, however, because the elastic joint reacts differently to a high-power input than it does to a low-power input. For the fixed-coefficient passive problem, different energy budgets will result in differently shaped gaits until the budget exceeds that of the maximum speed gait.

Although we cannot perform a simple time rescaling of a particular optimal gait for fixed-coefficient passive systems, we can examine the results of speed optimizations across different power budget allocations. In Figs. 9(a) and 9(b) we show optimization results for maximum possible speed across problems of constrained frequency and constrained maximum average power exertion. In these figures, each point on the greyscale surface is the result of an individual speed-optimization problem subject to the corresponding power and frequency constraints. The red curve represents the optimization problem of constrained power exertion while allowing the frequency to become an optimization variable. This line represents a Pareto frontier of optimal gaits over the two competing objective functions of gait speed and gait power consumption.

At low levels of power exertion, the motor cannot output enough acceleration to keep up with the best possible overall input frequency, so lower frequencies are more successful. As the power limit constraint is relaxed, the optimal frequency and speed increases until the maximum-speed frequency is reached. Past this point, increasing the power budget provides no benefit, as the motor is already capable of performing the maximum speed gait. Results for the fish-tail system are qualitatively identical to those of the three-link system.

IV. CONCLUSION

In this paper, we showed that geometric mechanics provides a computationally simple framework for finding optimal gaits in inertial systems with passive elements. We described a process for optimizing swimming system for cases where swimmer passive parameters can be optimized alongside swimmer gait motion and for cases where swimmer passive parameters are fixed in place. We believe that these tools can accelerate the design process for locomoting systems with passive-elastic components by identifying promising families of motion, and that this analysis provides fundamental intuition that can be useful for the development of such systems.

We considered two models of inertial swimming systems with passive-elastic components. We used the passive three-link swimmer as a simple model to discuss gaits that leverage passive dynamics to optimize swimmer behavior. Then, we presented a fish-tail swimmer to demonstrate how to geometrically represent continuously flexible systems and showed that this flexible swimmer leverages properties of motion that are qualitatively similar those used by the three-link swimmer.

By using passive parameters optimized for each system's unit-power limit cycle, we were able to generate the fairest possible comparison between the two systems, showing that a well-tuned fish-tail swimmer using our chosen curvature mode can be 20% faster than a well-tuned three-link swimmer at identical levels of power consumption.

For both of these swimming systems, we discussed results from optimizing with respect to three objective functions. We showed that optimizing with respect to speed produces a

single highest-speed gait consisting of a simple sinusoid that in cases of suboptimal passive properties is augmented with a small amount of high-order motion that has beneficial characteristics in the swimmer shape space. This maximum speed is limited by the passive dynamics of the swimmer: attempting to increase motor frequency beyond this point without change to passive coefficients elicits a response with poor behavior in shape space. We also show that efficiency objective functions that take into account only motor power consumption result in zero-motion optimal gaits that would not actually be useful for a swimmer attempting to travel between two points. This result aligns with our previous findings for passive swimmers in the drag-dominated regime [5]. Finally, for both classes of swimmer, we demonstrate that including metabolic overhead in the energy expenditure calculation results in a range of useful gaits that produce nontrivial efficient locomotion.

In future work, we intend to investigate selection of passive shape-modes that are most efficient for locomotion. Here, we assumed linearly varying mechanical properties across the length of our fish-tail swimmer, resulting in a particular passive shape mode that was more efficient than the three-link system. By intelligently choosing the moment of inertia of the tail along the backbone, we could attempt to design and optimize passive responses that are even more useful for locomotion. We also hope to examine swimmer locomotion in nonperfect fluids that allow for fluid drag and attempt to find optimal gaits for geometric swimming systems with both hydrodynamic mass and drag. Finally, we aim to extend this methodology to more complex systems, such as those with nonlinear springs that have been shown to have beneficial swimming properties in the past [22] or to systems with multiple active and passive shape modes, allowing for the modeling of traveling waves.

ACKNOWLEDGMENT

[1] D. N. Beal, F. S. Hover, M. S. Triantafyllou, J. C. Liao, and G. V. Lauder, Passive propulsion in vortex wakes, J. Fluid Mech. **549**, 385 (2006).

[2] T. McGeer, Passive dynamic walking, Int. J. Robot. Res. **9**, 62 (1990).

[3] T. Dear, B. Buchanan, R. Abrajan-Guerrero, S. D. Kelly, M. Travers, and H. Choset, Locomotion of a multi-link nonholonomic snake robot with passive joints, Int. J. Robot. Res. **39**, 598 (2020).

[4] T. Dear, S. D. Kelly, M. Travers, and H. Choset, Locomotive analysis of a single-input three-link snake robot, in *Proceedings of the IEEE 55th Conference on Decision and Control (CDC)* (IEEE, Piscataway, NJ, 2016).

[5] S. Ramasamy and R. L. Hatton, Optimal gaits for drag-dominated swimmers with passive elastic joints, Phys. Rev. E **103**, 032605 (2021).

[6] B. Bittner, R. L. Hatton, and S. Revzen, Data-driven geometric system identification for shape-underactuated dissipative systems, Bioinspir. Biomim. **17**, 026004 (2022).

[7] E. Kanso, J. E. Marsden, C. W. Rowley, and J. B. Melli-Huber, Locomotion of articulated bodies in a perfect fluid, J. Nonlin. Sci. **15**, 255 (2005).

[8] R. L. Hatton, Z. Brock, S. Chen, H. Choset, H. Faraji, R. Fu, N. Justus, and S. Ramasamy, The geometry of optimal gaits for inertia-dominated kinematic systems, IEEE Trans. Robot. **38**, 3279 (2022).

[9] R. L. Hatton and H. Choset, Geometric swimming at low and high Reynolds numbers, IEEE Trans. Robot. **29**, 615 (2013).

[10] C. Bass, S. Ramasamy, and R. L. Hatton, Characterizing error in noncommutative geometric gait analysis, in *Proceedings of the International Conference on Robotics and Automation (ICRA)* (IEEE, Piscataway, NJ, 2022).

[11] A. Abate, J. W. Hurst, and R. L. Hatton, Mechanical Antagonism in Legged Robots, in *Robotics: Science and Systems XII* (Robotics Science and Systems Foundation, San Francisco, CA, 2016).

[12] R. Hatton and H. Choset, Nonconservativity and noncommutativity in locomotion, Eur. Phys. J.: Spec. Top. **224**, 3141 (2015).

[13] R. L. Hatton and H. Choset, Geometric motion planning: The local connection, stokes' theorem, and the importance of coordinate choice, Int. J. Robot. Res. **30**, 988 (2011).

[14] E. M. Purcell, Life at low Reynolds number, Am. J. Phys. **45**, 3 (1977).

[15] J. N. Newman, *Marine Hydrodynamics* (MIT Press, London, UK, 2018).

[16] J. Sánchez-Rodríguez, F. Celestini, C. Raufaste, and M. Argentina, Proprioceptive mechanism for bioinspired fish swimming, Phys. Rev. Lett. **126**, 234501 (2021).

[17] G. V. Lauder, B. Flammang, and S. Alben, Passive robotic models of propulsion by the bodies and caudal fins of fish, Integr. Compar. Biol. **52**, 576 (2012).

[18] S. N. H. Syuhri, D. Pickles, H. Zare-Behtash, and A. Cammarano, Influence of travelling waves on the fluid dynamics of a beam submerged in water, J. Fluids Struct. **121**, 103947 (2023).

[19] S. Ramasamy and R. L. Hatton, The geometry of optimal gaits for drag-dominated kinematic systems, IEEE Trans. Robotics **35**, 1014 (2019).

[20] G. J. Stephens, B. Johnson-Kerner, W. Bialek, and W. S. Ryu, Dimensionality and dynamics in the behavior of C. elegans, PLoS Comput. Biol. **4**, e1000028 (2008).

[21] M. Sfakiotakis, D. Lane, and J. Davies, Review of fish swimming modes for aquatic locomotion, IEEE J. Ocean. Eng. **24**, 237 (1999).

[22] M. Sharifzadeh and D. M. Aukes, Curvature-induced buckling for flapping-wing vehicles, IEEE/ASME Trans. Mechatron. **26**, 503 (2021).